Section 9

Development of and studies with coupled and Earth system models and data assimilation systems.

Model Development of the Unified Forecast System for Subseasonal to Seasonal Timescales

Jessica Meixner[1,*], Lydia Stefanova[2], Denise Worthen[2], Jiande Wang[2], Jun Wang[1], Shrinivas Moorthi[1], Bin Li[2], Jian Kuang[2], Robert Grumbine[1], Arun Chawla[1], Avichal Mehra[1]

[1]NOAA/NWS/NCEP/EMC [2]IMSG at NOAA/NWS/NCEP/EMC

*Jessica.Meixner@noaa.gov

Introduction

In response to the Weather Research and Forecasting Innovation Act of 2017, NCEP is developing a seasonal to subseasonal forecast model utilizing the Unified Forecast System. The Unified Forecast System is a community based coupled earth system model with applications from regional to global scales and from weather to climate timescales. This coupled model development is actively underway at NCEP and the first operational goal for the fully coupled atmosphere-ocean-ice-wave model will be the Global Ensemble Forecasting System GEFSv13 in FY2023, followed by a seasonal forecasting system in FY2025. Here we will describe the current state of the subseasonal to seasonal coupled model, provide selected results to demonstrate progress and discuss future plans.

Model Description

For the subseasonal to seasonal timescales we are employing an atmospheric model with the Finite Volume Cubed Sphere (FV3) dynamical core with GFS physics and GFDL microphysics, the Modular Ocean Model (MOM6) and the Los Alamos Sea Ice Model (CICE5). These models are coupled together using the NOAA Environmental Modeling System (NEMS) which currently contains both a driver and a mediator. The coupling infrastructure is built employing the National Unified Operational Prediction Capability (NUOPC) Layer [Theurich, 2016] on top of the Earth System Modeling Framework (ESMF).

For the results here, the atmospheric model uses the C384 cubed sphere grid (~25km) with 64 layers. The ocean model employs a ¼° tripolar grid with 75 hybrid coordinate layers following the OM4.0 setup [Adcroft, 2019]. The ice model uses the same tripolar grid as the ocean and does not use Mushy thermodynamics. In the current implementation using the NEMS mediator, atmosphere/ice fluxes are computed by the ice model and atmosphere/ocean fluxes are computed by the atmospheric model. The atmospheric model's land/sea mask does not match the ocean/ice mask and does not permit fractional land masks. For interpolating the sea surface temperature from the ocean to the atmosphere, a conservative interpolation is used and then if a valid temperature is not obtained, nearest neighbor is used to fill remaining non-land points. The fluxes received by the ocean model are a combination of the fluxes computed by the atmosphere and ice weighted by the ice fraction.

Results

Development is actively ongoing, however, our intermediate results show great promise for the future operational systems. For brevity just the ice area in the Arctic for 2017 is shown in Figure 1. This compares two different UFS prototypes showing the impacts of initial conditions, comparing CFSR (UFS_p2) versus CPC ice analysis (UFS_p3) initial conditions. The atmosphere is also initialized by CFSR and the ocean model is initialized from the CPC 3Dvar analysis for both prototypes. Initial assessments of all UFS prototypes have shown skill improvement over CFSv2 for all components, including improvement of predictions for ice concentration, area, and extent in the polar regions.

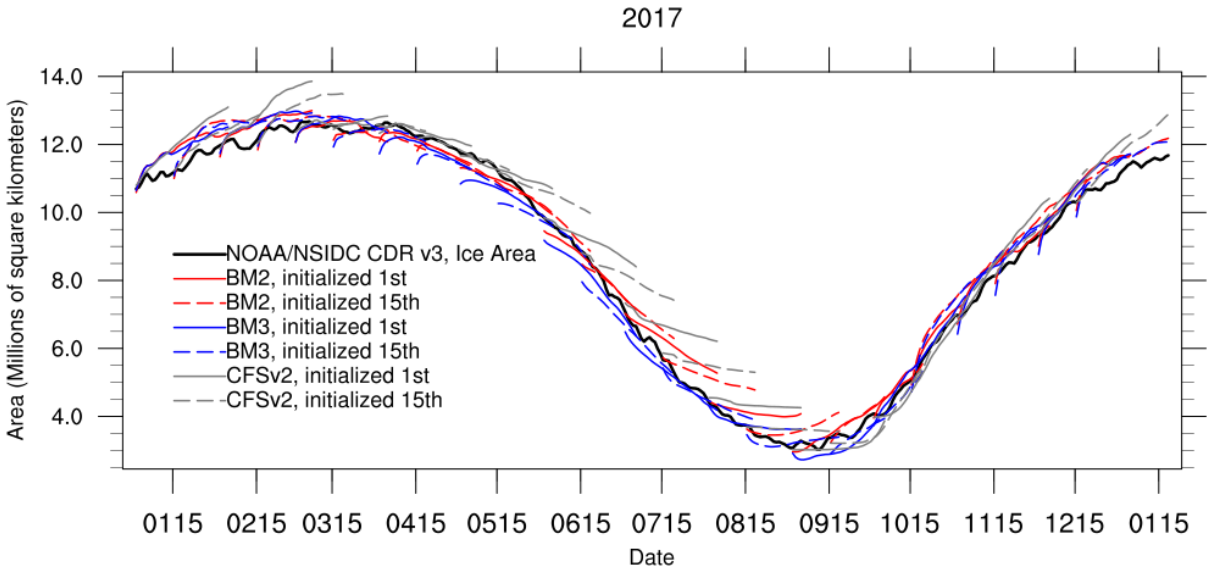

Figure 1. This figure shows the ice area for the year 2017 for the Arctic comparing two different UFS prototypes (UFS_p2, UFS_p3), with CFSv2, and NOAA/NSIDC CDR v3 ice area (https://nsidc.org/data/g02202/versions/3).

Future Developments

Model and engineering development activities are actively ongoing. Future engineering development activities will include transitioning to the Common Community Physics Package (CCPP) for the atmospheric model and to the Community Mediator for Earth Prediction Systems (CMEPS) for the mediator. Future planned model developments include adding the wave model WAVEWATCH III, to add sea-state dependent roughness back to the atmosphere and to include sea-state dependent Langmuir mixing in the ocean. Additional improvements will include updates to the GFSv16 atmosphere component with increased vertical resolution, model physics tuning, and data assimilation.

References

Adcroft, A., Anderson, W., Balaji, V., Blanton, C., Bushuk, M., Dufour, C. O., et al. (2019). The GFDL global ocean and sea ice model OM4.0: Model description and simulation features. *Journal of Advances in Modeling Earth Systems*, 11, 3167– 3211. https://doi.org/10.1029/2019MS001726

Theurich, G., C. DeLuca, T. Campbell, F. Liu, K. Saint, M. Vertenstein, J. Chen, R. Oehmke, J. Doyle, T. Whitcomb, A. Wallcraft, M. Iredell, T. Black, A.M. Da Silva, T. Clune, R. Ferraro, P. Li, M. Kelley, I. Aleinov, V. Balaji, N. Zadeh, R. Jacob, B. Kirtman, F. Giraldo, D. McCarren, S. Sandgathe, S. Peckham, and R. Dunlap, 2016: The Earth System Prediction Suite: Toward a Coordinated U.S. Modeling Capability. Bull. *American Meteorological Society*, 97, 1229–1247, https://doi.org/10.1175/BAMS-D-14-00164.1

Acknowledgements

This project is part of a community effort and would not be possible without the contributions from our collaborators and we are extremely grateful for our colleagues at NOAA/OAR/GFDL, NOAA/OAR/ESRL, UCAR/NCAR and more.

Relation between Eurasian snow and India monsoon in historical simulation of CMIP5 models

Amita Prabhu[1] and Sujata K. Mandke[1,*]

[1]Indian Institute of Tropical Meteorology, Ministry of Earth Sciences, INDIA

amitaprabhu@tropmet.res.in, *amin@tropmet.res.in

Introduction

Observations have lend credence to the Eurasian winter/spring snow relation with the following summer monsoon rainfall over India. Next question arises - Whether state-of-the-art atmosphere-ocean coupled models have skill to simulate this snow-monsoon relation. To answer this question, our aim is to examine the fidelity of the global coupled climate models from Coupled Model Intercomparison Project 5 (CMIP5; Taylor et al., 2012) to simulate snow-monsoon relation. Historical simulations of five CMIP5 coupled models (CCSM4, CNRM-CM5, GFDL-ESM2G, MIROC4h, NorESM1-M) are selected for the study, based on their skill in terms of highest skill scores for greater number of diagnostics to simulate Asian summer monsoon climatology and climatological annual cycle (Sperber et al. 2013).

Data

Model: Monthly mean precipitation and snowfall flux of five models (Table 1) from 20th century historical simulation of CMIP5 (http://www-pcmdi.llnl.gov) are used. **Observation**: (i) Daily rainfall data developed by India Meteorological Department (Pai et al.. 2014), across the Indian landmass (ii) National Snow and Ice Data Center archived snow water equivalent data from Scanning Multichannel Microwave Radiometer (SMMR) and Special Sensor Microwave/Imager (SSM/I).

Table 1: CMIP5 models used in the present study (atmospheric horizontal resolution (in °E X °N))

No.	Model name	Atmosphere horizontal resolution
1.	CCSM4	1.2x0.9
2.	CNRM-CM5	1.4x1.4
3.	GFDL-ESM2G	2.5x2.0
4.	MIROC4h	T213L56
5.	NorESM1-M	2.5x1.9

Results

Correlation coefficient (CC) between summer monsoon rainfall at each grid point over the Indian landmass with the preceding winter season snow averaged over Eurasia (50-70°N, 20-140°E), using observed data is illustrated (Figure 1a). The average of four months from December of previous year to March of the following year is referred as winter season and June to September average as summer monsoon season. Similar CC between precipitation at each grid point over India and neighboring oceans with the preceding winter Eurasian snow is also analyzed for historical simulation of five CMIP5 models (Figures 1(b-f)) respectively. A close examination of observed CC (Fig. 1a) reveals a 'Negative-Positive-Negative' tri-polar spatial pattern. Clusters of significant negative CC over the northern (~ 35°N, 78°E) and south-western (~ 20°N, 75°E) boundary of India, while positive CC over east-central (~ 26°N, 82°E) regions of India with slight positive traces over Northeast India are evident. The major differences between spatial patterns of CC in observation (Fig. 1a) and models (Fig. 1(b-d) are due to the large differences in their spatial resolution, with very high resolution of observed data compared to models. However, among five models, regional features of CC in CCSM4 model are closer to observation with similar tri-polar pattern, while other four models are far from observation. Positive (negative) CC over large portion of Indian land is noticed in MIROC4h (NORESM1-M) model.

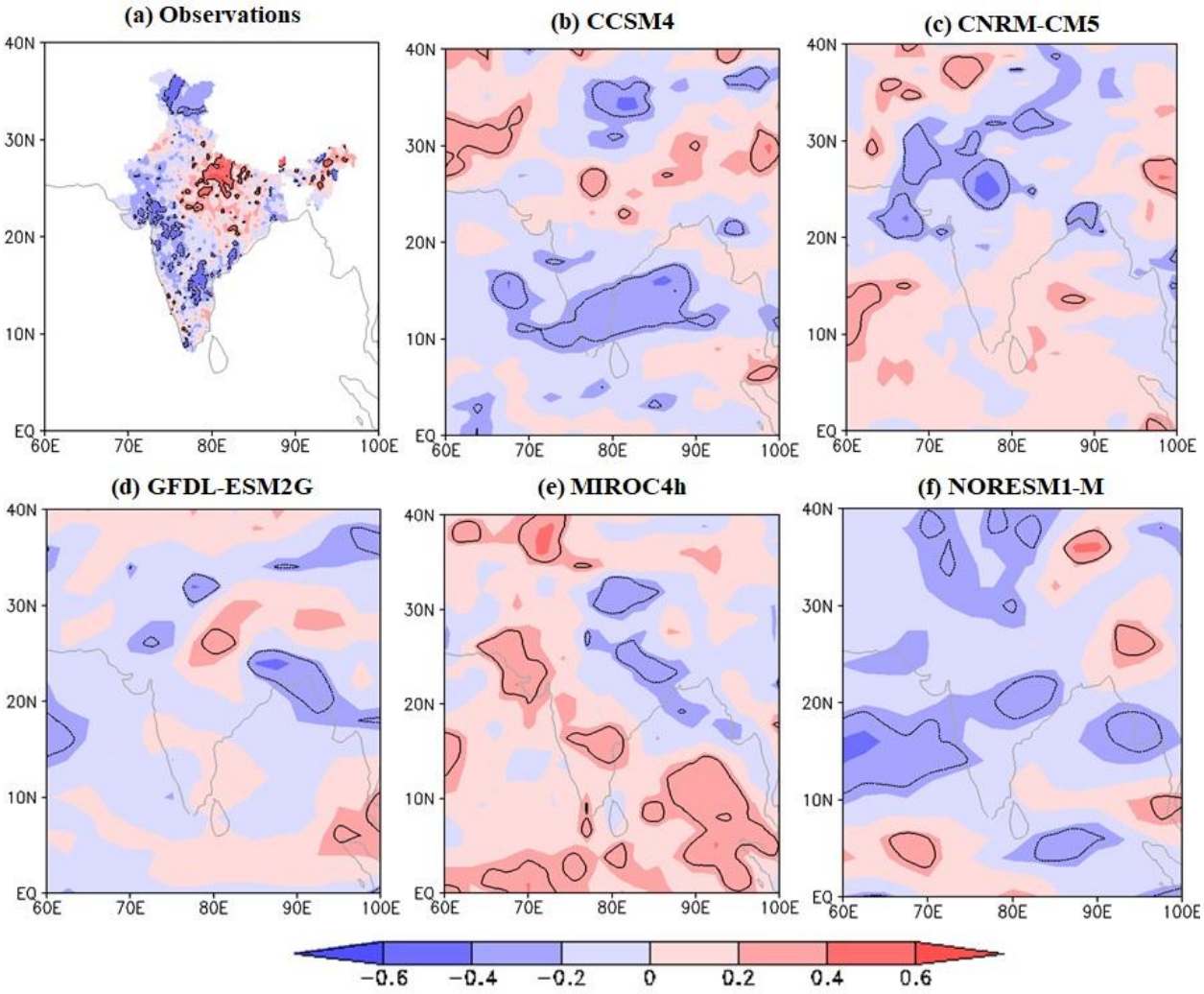

Figure 1(a-f): Correlation coefficient (shaded) of summer monsoon precipitation at each grid point over the Indian domain with the preceding winter snow averaged over Eurasia, for observation and five CMIP5 models respectively. Black solid contours represent significance at 95% confidence level.

References

Pai DS, Sridhar L, Rajeevan M, Sreejith OP, Satbhai NS, Mukhopadhyay B.,2014. Development of a new high spatial resolution (0.25 × 0.25 degree) long period (1901–2010) daily gridded rainfall data set over India and its comparison with existing data sets over the region. Mausam 65(1):1–18

Sperber, K.R., Annamalai, H., Kang, I.S., Kitoh, A., Moise, A., Turner, A., Wang, B., Zhou,T., 2013. The Asian summer monsoon: an intercomparison of CMIP5 vs. CMIP3 simulations of the late 20th century. Clim.Dyn. 41, 2711–2744.http://dx.doi.org/10.1007/s00382-012-1607-6

Taylor K.E., Stouffer R.J. and Meehl G.A. .2012. An overview of CMIP5 and the experiment design, Bull. Amer. Meteorol. Soc, 90,4 :85–498.

Atmosphere-wave-ocean coupled-model simulation on Typhoon Bualoi(2019) and formation of quasi-linear convective system around Boso Peninsula

Akiyoshi Wada

[1]Meteorological Research Institute, Tsukuba, Ibaraki, 305-0052, JAPAN

[1]awada@mri-jma.go.jp

1. Introduction

On October 25 in 2019, heavy rainfall accompanied by low pressure was observed on the Boso Peninsula (Fig. 1), causing serious natural disasters when Typhoon Bualoi was transited into an extratropical cyclone east of Japan. Although the warm and moist air transported from this typhoon is thought to be one of the factors in formation of the convection system and heavy rainfall, the relationship is not clear. In order to understand the role of the ocean in the simulations of Bualoi and formation of the convective system, numerical simulations were performed by using a coupled atmosphere-wave-ocean model (Wada et al., 2018).

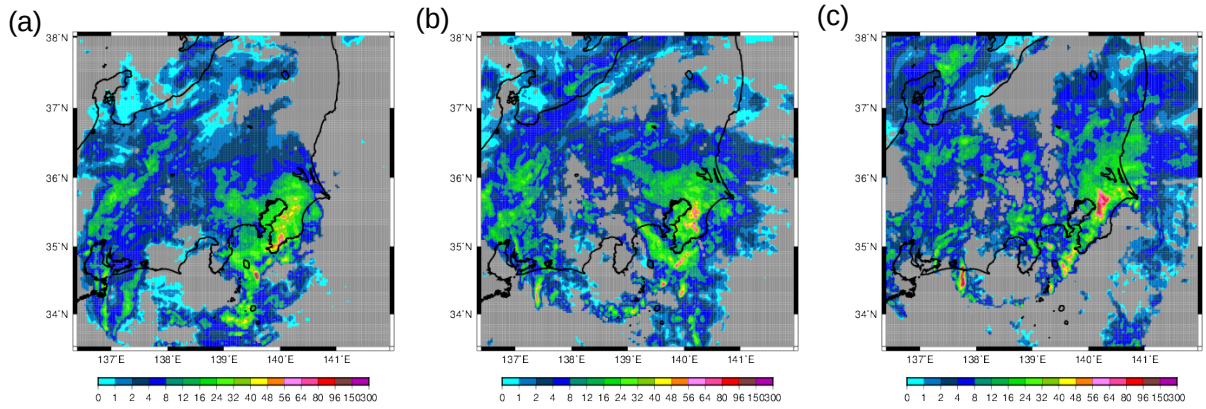

Figure 1 The 1-hour rainfall distribution analyzed every 10 minutes (mm/hour) at (a) 00 UTC, (b) 02 UTC and (c) 04 UTC on 25 October in 2019.

2. Experimental design

The list of numerical simulations is shown in Table 1. Each initial time was 0000 UTC on October 22. The computational domain was 2160 x 4320 km. The number of the vertical layer was 55. The top height was approximately 27 km. The integration time was 36 hours. The time step was 3 seconds for NHM, 18 seconds for the ocean model, and 6 minutes for the ocean surface wave model. The physical components were exchanged between NHM, the ocean model, and the ocean surface wave model every time step of a model with a longer time step. The Japan Meteorological Agency (JMA) global objective analysis with horizontal resolution of 20 km and the JMA North Pacific Ocean analysis with horizontal resolution of 0.5° were used for creating atmospheric and oceanic initial conditions and atmospheric lateral boundary conditions. In addition, climatological oceanic averaged data are calculated by using the oceanic reanalysis data from 1982 to 2018 (Usui et al., 2017). When the climatological data are used in the simulation, 'AVE' is added to the end of the experiment name shown in Table 1.

Table1 List of numerical simulations

Name	***Model***	***Ocean***
NHM	NHM	2019
CPL	Coupled NHM-wave-ocean model	2019
NHMAVE	NHM	Climatology
CPLAVE	Coupled NHM-wave-ocean model	Climatology

3. Results

3.1 Track and central pressure

Figure 2 shows the simulated track of Bualoi and time series of simulated central pressure with the best track data. The track was reasonably simulated. Increases in central pressure during the decaying phase was also reasonably simulated although the initial value was quite different between best track data and simulation results. The effect of

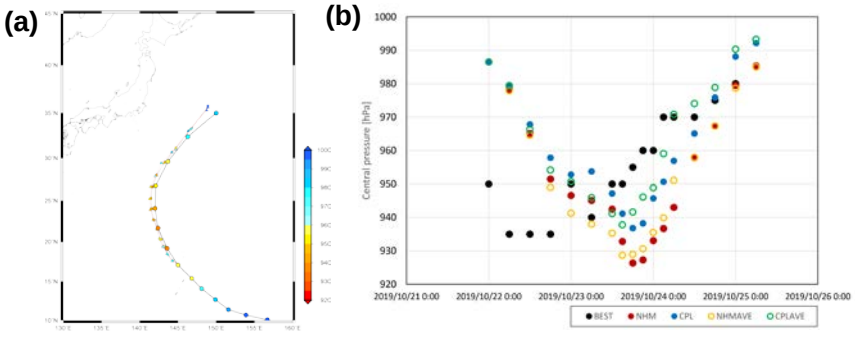

Figure 2 (a) The simulated track of Bualoi with the best track. Squares indicate the result of NHM and triangles indicate the result of the coupled model. The red line shows the result of climatological oceanic condition. The color shows the value of the central pressure. (b) Time series of simulated central pressure with the best-track central pressure.

ocean coupling and preexisting oceanic condition on the simulations was found in the values of simulated minimum central pressure and simulated central pressure during the decaying phase.

3.2 Rainfall distribution

Figure 3 shows the horizontal distributions of accumulated rainfall for 90 hours in the four experiments (Table 1). There is no essential difference between the four accumulated precipitation distributions. However, in the CPL experiment, the accumulated rainfall was higher in Boso Peninsula than in the other experiments. It should be noted that the maximum accumulated precipitation did not always decrease by ocean coupling or by the use of climatological mean oceanic initial condition in spite that they did affect typhoon intensity simulation directly.

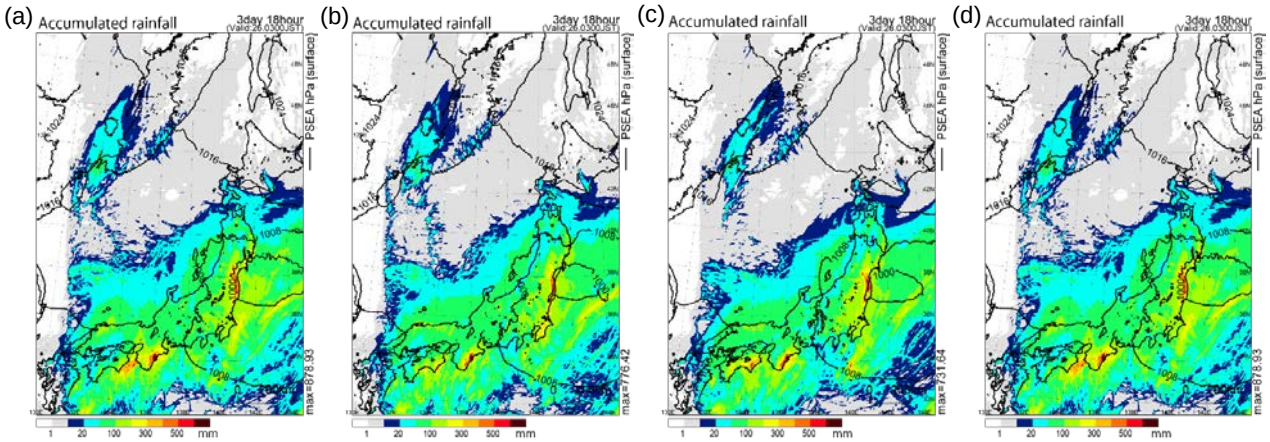

Figure 3 Accumulated rainfall distribution for 90 hours in the (a) NHM, (b) CPL, (c) NHMAVE and (d) CPLAVE experiments.

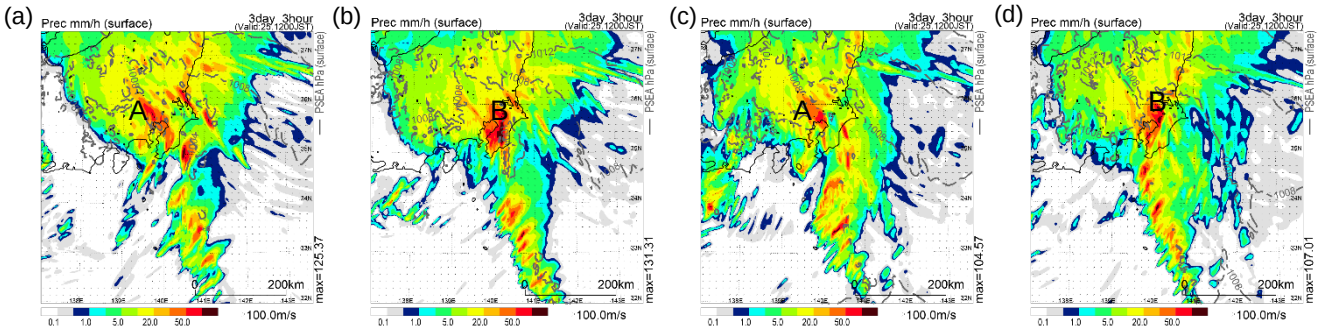

Figure 4 Accumulated 1-hour rainfall distribution (mm/hour) at 03 UTC (12 JST) on October 25 in the (a) NHM, (b) CPL, (c) NHMAVE and (d) CPLAVE experiments.

Figure 4 shows the horizontal distribution of simulated accumulated 1-hour rainfall in the four experiments. Differently from the results shown in Fig. 3, the distribution of local convective system was greatly different between the four experiments. Around the Boso Peninsula, some experiments (‘A’ in Fig. 4a,c) showed that the northwest-southeast precipitation system was dominant, while the others (‘B’ in Fig. 4b,d) showed the north-south quasi-linear convection system on the Boso Peninsula. This suggests that the ocean coupling may affect the simulation of local precipitation system caused in the Boso Peninsula although the precipitation pattern on a synoptic scale was almost the same between the four experiments.

4. Concluding remarks

The effects of ocean coupling and preexisting oceanic condition did affect the simulated central pressure of Bualoi and the convective precipitation system on the Boso Peninsula. In contrast, it had a small impact on the rainfall distribution on a synoptic scale. It should be noted that this result may be affected by the constraints of lateral boundary conditions that are unique to numerical simulations using regional atmosphere models.

References

Usui, N, T. Wakamatsu, Y. Tanaka, N. Hirose, T. Toyoda, S. Nishikawa, et al, (2017), Four-dimensional variational ocean reanalysis: a 30-year high-resolution dataset in the western North Pacific (FORA-WNP30). Journal of Oceanography, 73, 205-233.

Wada, A., S. Kanada, and H. Yamada (2018). Effect of air–sea environmental conditions and interfacial processes on extremely intense typhoon Haiyan (2013). Journal of Geophysical Research: Atmospheres, 123, 10379-10405.

The effect of the cloud-water conversion rate in the cumulus parameterization on the simulation of Typhoon Lionrock (2016)

Akiyoshi Wada*, Hiromasa Yoshimura and Masayuki Nakagawa
Meteorological Research Institute, Tsukuba, Ibaraki, 305-0052, JAPAN
*awada@mri-jma.go.jp

1. Introduction

Wada et al. (2019) performed numerical simulations of Typhoon Lionrock (2016) using the 7-km mesh nonhydrostatic global spectral atmospheric Double Fourier Series Model (DFSM) (Nakano et al., 2017) coupled with the MRI Community Ocean Model Version 4.4 (MRI.COM) and showed that the simulated typhoon track greatly changed due to the effect of ocean coupling when the cumulus parameterization was used in DFSM. The purpose of this study is to understand the effect of the cumulus parameterization on the typhoon track simulation in a coupled atmosphere and ocean framework, and to improve the typhoon track simulation. We investigated the impact of the rate (hereafter referred as 'rtau') that adjusts the conversion from cloud water to precipitation during the updraft of cumulus on the simulation of Lionrock. The smaller rtau is, the smaller the conversion rate from cloud water to precipitation is. The reduction in the conversion rate is expected to contribute to increases in the number of tall cumulus due to increases in latent heat release of cloud ice without falling directly below, to increases in the cloud amount detrained from the cloud top, and to decreases in the amount of precipitation converted from cumulus.

2. Experimental design

The experimental design is almost the same as Wada et al. (2019). The list is shown in Table 1. The initial time of the simulation of Lionrock is set to 0000 UTC on August 23 in 2016. The period is from this initial time to 0000 UTC on August 31 in 2016. The integration time is 8 days. The DFSM and MRI.COM used in this study are the same as Wada et al. (2019). The Japan Meteorological Agency 6-hourly global objective analysis data are used for each experiment to create atmospheric initial conditions (Nakano et al., 2017). In addition, the global ocean reanalysis data are used for each experiment to create oceanic initial conditions (Toyoda, private communication).

Table 1 List of sensitivity numerical experiments for the prediction of Lionrock

Experiment name	OCEAN	rtau (1/m)
ASM_CNTL	SST	4.0d-3
CASM_CNTL	Couple	4.0d-3
ASM_RT_S	SST	4.0d-5
CASM_RT_S	Couple	4.0d-5

3. Results

3.1 Track and SST simulations

Figure 1a-b shows the horizontal distributions of simulated sea surface temperature in the (a) CASM_CNTL and (b) CASM_RT_S experiments together with the simulated tracks and the Regional Specialized Meteorological Center Tokyo best-track. Both experiments showed that Lionrock-induced sea surface cooling is caused beneath the typhoon around the recurvature area. However, after the recurvature, the sea surface cooling is induced along the right side of the track only in the CASM_CNTL experiment. Sea surface cooling in Fig. 1b is relatively small compared with the analyzed sea surface temperature field (Fig. 1d in Wada et al., 2019). The large differences in simulated tracks between the ASM_CNTL and CASM_CNTL experiments in Fig. 1a becomes small in Fig. 1b. It is suggested the simulated tracks affected by ocean coupling are improved by adjusting the parameter rtau when the cumulus parameterization is used.

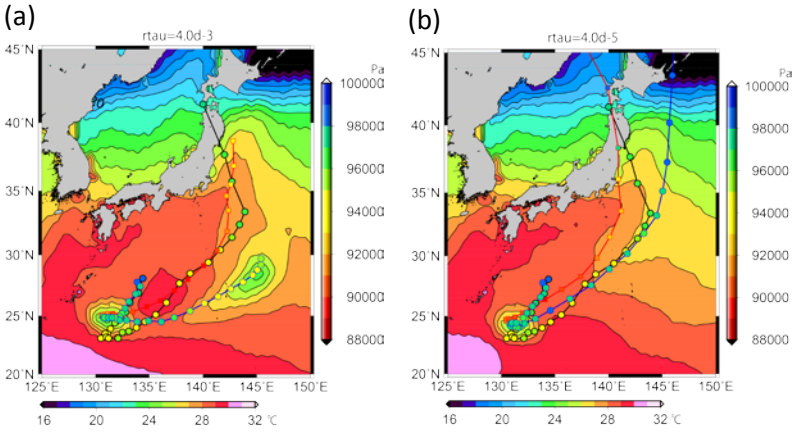

Figure 1 Horizontal distributions of simulated sea surface temperature in (a) CASM_CNTL and (b) CASM_RT_S (colors with the contours (1 ℃) at 0000 UTC on August 31 in 2016 with the best track (black line: the color within a circle indicates central pressures) and simulated tracks (red: results by DFSM alone, blue: results by the coupled model) in (a) ASM_CNTL and CASM_CNTL experiments and in (b) ASM_RT_S and CASM_RT_S experiments.

3.2 Intensity simulations

Figure 2 shows the time series of best-track and simulated central pressures in the (a) ASM_CNTL and CASM_CNTL and (b) ASM_RT_S and CASM_RT_S experiments. Minimum central pressure in the ASM_RT_S (CASM_RT_S) experiment is higher than that in the ASM_CNTL (CASM_CNTL) experiments. The relatively weak intensity in the CASM_RT_S experiment leads to relatively small sea surface cooling along the right side of the track after the recurvature of simulated Lionrock. The result suggests that improving the typhoon track simulation does not lead to the improvement of the typhoon intensity simulation.

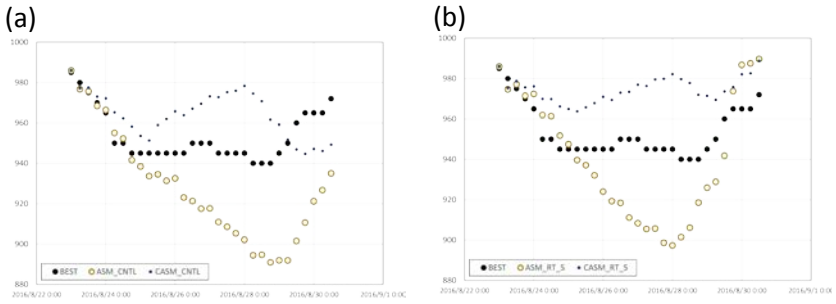

Figure 2 Time series of best-track (BEST) and simulated central pressures in (a) ASM_CNTL and CASM_CNTL and (b) ASM_RT_S and CASM_RT_S experiments.

3.3 Sea surface temperature and precipitable water

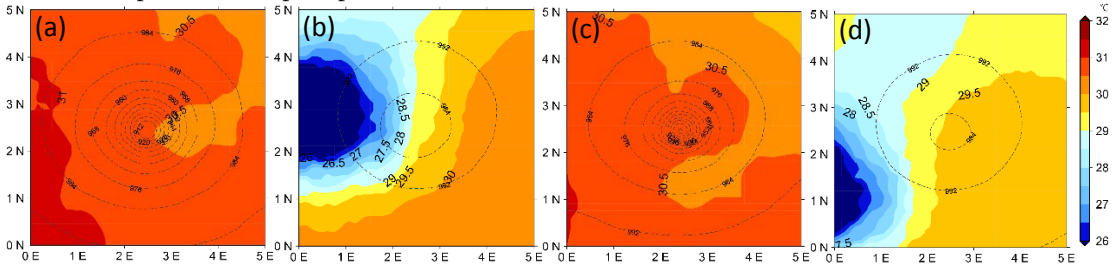

Figure 3 Horizontal distributions of sea surface temperature (shades) collocated at the simulated storm center at the 120-h integration time in the (a)ASM CNTL, (b) CASM CNTL, (c) ASM RT S and (d) CASM RT S experiments.

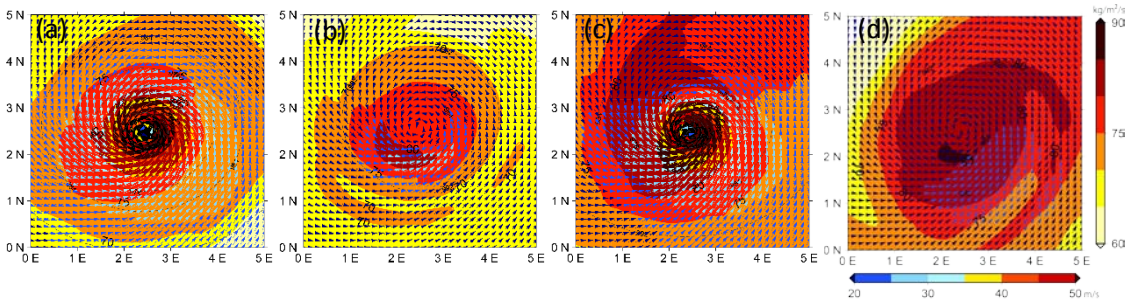

Figure 4 Horizontal distributions of precipitable water (shades: color bar is shown in the right side) together with the surface wind vector (color bar is shown on the lower side) collocated at the predicted storm center at the 120-h integration time in the (a)ASM_CNTL, (b) CASM_CNTL, (c) ASM_RT_S and (d) CASM_RT_S experiments.

Figure 3 shows the horizontal distribution of sea surface temperature around the simulated typhoon center at the 120-h integration time. In the ASM_CNTL experiment, the location of the typhoon is more southward compared with the location in the ASM_RT_S experiment although the difference of the value of simulated sea surface temperature is relatively small compared with the difference between CASM_CNTL and CASM_RT_S experiments. In the CASM_RT_S experiment, sea surface temperature underneath the simulated typhoon is relatively high compared with that in the CASM_CNTL experiments. In fact, the area of relatively strong surface wind speeds southeast of the typhoon center in the CASM_RT_S is wider than that south of the typhoon center in the CASM_CNTL experiment. The inner-core structural change caused by the change in the value of rtau in the cumulus parameterization may be related to the change in the track simulation in the coupled atmosphere-ocean framework.

4. Concluding remarks

This study confirmed that changing one parameter 'rtau' (the rate that adjusts the conversion from cloud water to precipitation) in the cumulus parameterization leads to the inner-core structural change of simulated typhoon, differences in the amount of precipitable water, and changes in the track simulation. However, the simulated typhoon intensity is not still accurate compared with the best track analysis. Nevertheless, this study implies that the improvement of cumulus parameterization certainly plays a key role to improve the typhoon prediction in the coupled atmosphere-ocean framework.

References

Nakano, M., A. Wada, M. Sawada, H. Yoshimura, R. Onishi, S. Kawahara, W. Sasaki, T. Nasuno, M. Yamaguchi, T. Iriguchi, M. Sugi, and Y. Takeuchi, (2017). Global 7 km mesh nonhydrostatic Model Intercomparison Project for improving TYphoon forecast (TYMIP-G7): experimental design and preliminary results. Geosci. Model Dev., 10, 1363-1381, https://doi.org/10.5194/gmd-10-1363-2017

Wada, A., H. Yoshimura, M. Nakagawa.（2019) Preliminary numerical experiments on the prediction of Typhoon Lionrock (2016) using the global atmosphere-ocean coupled model. CAS/JSC WGNE Res. Activities in Atm. And. Oceanic Modelling. Rep.49, 9-05.

Rainfall simulations of Typhoons Kammuri and Phanfone landfalling in the Philippines

Akiyoshi Wada

[1]Meteorological Research Institute, Tsukuba, Ibaraki, 305-0052, JAPAN

[1]awada@mri-jma.go.jp

1. Introduction

In the Philippines, 4-5 typhoons make landfall in a year on average. In 2019, five typhoons made landfall in the Philippines. Heavy rain and strong winds associated with the typhoons often cause natural disasters in the Philippines. Wada and Gile (2019) showed that cumulation parameterization in a nonhydrostatic atmospheric model (NHM) is required to accurately simulate the distribution of rainfall associated with a typhoon. However, other factors affecting rainfall simulations such as the mutual effect between ocean coupling and cloud physics have not been investigated so far. The purpose of this study is to investigate the effects of ocean coupling and inhibition rates of evaporation of rain, snow and graupel included in the cloud physics on the rainfall simulation in the cases of Typhoon Kammuri and Phanfone using the NHM coupled with the multilayer ocean model and the third-generation ocean surface wave model (CPL) (Wada et al., 2010, 2018).

2. Experimental design

The list of numerical simulations is shown in Table 1. Each initial time was 0000 UTC on November 27 for Kammuri and 0000 UTC on December 23. The computational domain was 4800 x 2400 km for Kammuri's simulation and 2700 x 2400 km for Phanfone's simulation. The number of the vertical layer was 55. The top height was approximately 27 km.

Table1 List of numerical simulations

Name	***Model***	***Evaporation Inhibition Rate***	***Typhoon cases***
NHM EVP0	NHM	0	Kammuei (2019/11/27/0000)
CPL EVP0	Coupled NHM-wave-ocean model	0	
NHM EVP1	NHM	1	Phanfone (2019/12/23/0000)
CPL EVP1	Coupled NHM-wave-ocean model	1	

The integration time was 168 hours for Kammuri and 72 hours for Phanfone. The time step was 3 seconds for NHM, 18 seconds for the ocean model, and 6 minutes for the ocean surface wave model. The physical components were exchanged between NHM, the ocean model, and the ocean surface wave model every time step of a model with a longer time step. The Japan Meteorological Agency (JMA) global objective analysis with horizontal resolution of 20 km and the JMA North Pacific Ocean analysis with horizontal resolution of 0.5° were used for creating atmospheric and oceanic initial conditions and atmospheric lateral boundary conditions. In addition, climatological oceanic averaged data are calculated by using the oceanic reanalysis data from 1982 to 2018 (Usui et al., 2017). When the climatological data are used in the simulation, 'AVE' is added to the end of the experiment name shown in Table 1. Tropical Cyclone Database (https://sharaku.eorc.jaxa.jp/TYP_DB/index_e.html) is used to obtain the Global Precipitation Measurement (GPM) Microwave Imager (GMI) and the Dual-frequency Precipitation Radar (DPR) data,

3. Results

3.1 Kammuri

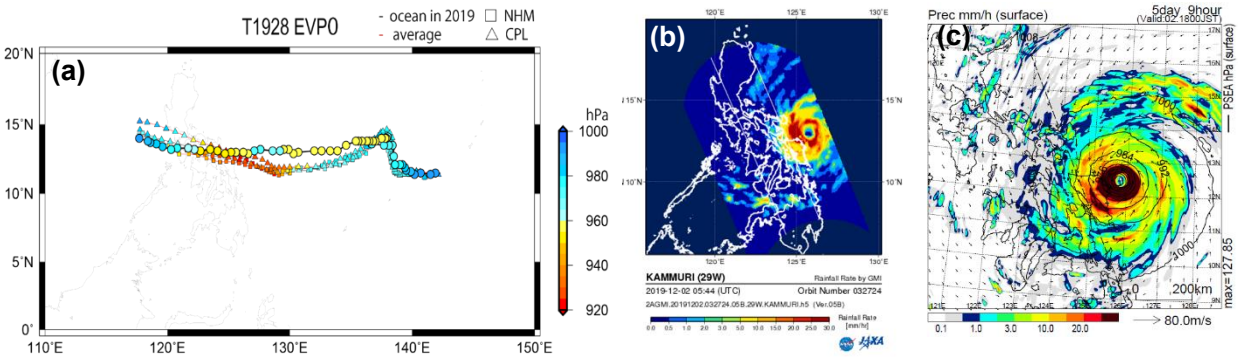

Figure 1 (a) Early analysis on the track and central pressure (hPa) of Typhoon Kammuri and simulation results. (b) Horizontal distribution of hourly rainfall obtained from GMI. (c) Horizontal distribution of simulated hourly rainfall at the 129-hour integration time in the CPL EXP0 experiment.

Figure 1a shows the results of track and central pressure simulations together with the results of early analysis. The tracks in the four experiments with the inhibition rate of 0.0 are reasonably simulated compared with the early

analysis. However, the simulated central pressures are relatively low around 125-130˚E before making landfall in the Philippines. In fact, the hourly rainfall distribution obtained from GMI shows the robustness of the eyewall (Fig. 1b). In addition, a primary rainband is remarkable along the eastern coast of the Samar island. The simulation result in the CPL EXP0 experiment captures these features to some extent (Fig. 1c). The effect of oceanic initial conditions on the intensity and rainfall distribution is relatively small compared with that of ocean coupling (not shown).

3.2 Phanfone

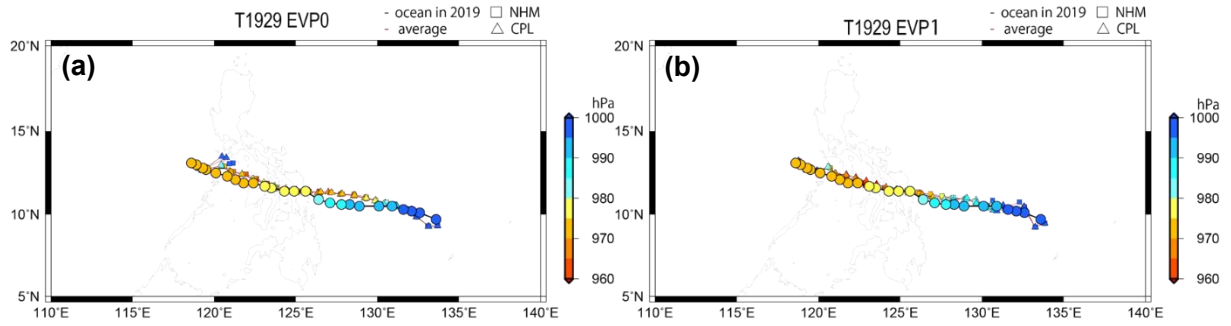

Figure 2 Early analysis on the track and central pressure (hPa) of Typhoon Phanfone and simulation results (a) in the EVP0 experiments and (b) in the EVP1 experiments.

Figure 2 shows the results of track and central pressure simulations together with the results of early analysis in the EVP0 (Fig. 2a) and EVP1(Fig. 2b) experiments. The difference of the inhibition rate slightly affects the simulated track. The change in the track simulation also affects the evolution of central pressure simulations. In this case, the effect of oceanic initial conditions on the intensity and rainfall distribution is also relatively small compared with that of ocean coupling (not shown). This suggests that ocean coupling is the most crucial process for improving the simulation of hourly rainfall distribution.

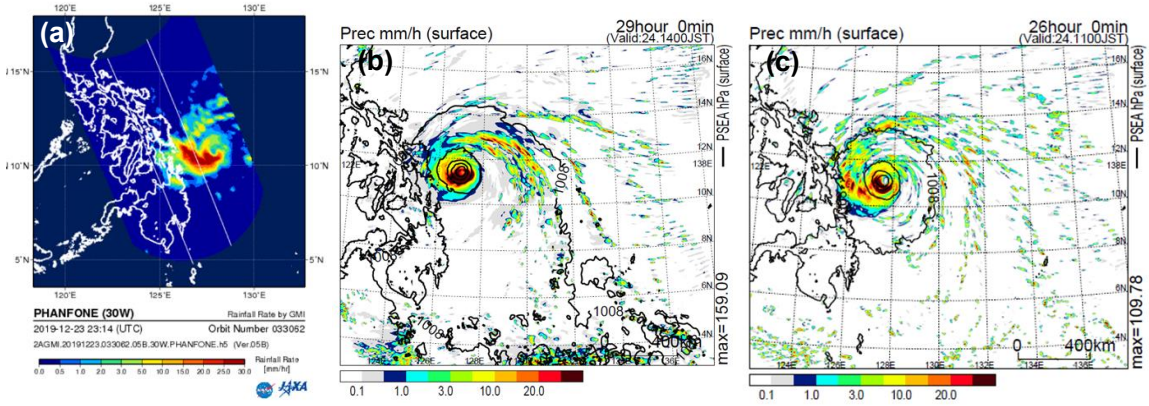

Figure 3 (a) Horizontal distribution of hourly rainfall of Typhoon Phanfone obtained from GMI. (b,c) Horizontal distribution of simulated hourly rainfall (B) at the 29-hour integration time in the CPL EXP0 experiment and (c) at the 26-hour integration time in the CPL EXP1 experiment .

Figure 3 shows the horizontal distribution of analyzed and simulated hourly rainfall. The pattern consists of broad primary rainband south of the typhoon center and relatively narrow spiral rainbands north of the center. When the inhibition rate of evaporation is set to be 0.0, these two features are not clear, and the pattern becomes more concentric. The two features are reasonably simulated when the inhibition rate of evaporation is set to be 1.0. The results suggest that the setting of the inhibition rate is important to simulate the hourly rainfall distribution in addition to ocean coupling.

4. Future study

It is possible to specify the optimal parameters regarding the inhibition rate of evaporation by verifying the simulation results with the DPR data in a 3-dimentional view. This is one of the plans in the future.

References

Usui, N, T. Wakamatsu, Y. Tanaka, N. Hirose, T. Toyoda, S. Nishikawa, et al, (2017), Four-dimensional variational ocean reanalysis: a 30-year high-resolution dataset in the western North Pacific (FORA-WNP30). Journal of Oceanography, 73, 205-233.

Wada, A. and R.P.Gile (2019). Roles of ocean coupling and cumulus parameterization in predicting rainfall amounts caused by landfalling typhoons in the Philippines. 49. 9.07-9.08.

Wada, A., S. Kanada, and H. Yamada (2018). Effect of air–sea environmental conditions and interfacial processes on extremely intense typhoon Haiyan (2013). Journal of Geophysical Research: Atmospheres, 123, 10379-10405.

Sensitivity experiments on axisymmetrization of Typhoon Faxai (2019) just before landfalling in Japan simulated by atmosphere-ocean coupled model

Akiyoshi Wada

[1]Meteorological Research Institute, Tsukuba, Ibaraki, 305-0052, JAPAN

[1]awada@mri-jma.go.jp

1. Introduction

Typhoon Faxai (2019) made landfall in Chiba Prefecture on September 9, causing a serious disaster mainly in the Boso Peninsula. When the typhoon entered Tokyo Bay from Sagami Bay, the 1-hour rainfall distribution analyzed every 10 minutes showed the structural change from the symmetric to axisymmetric pattern (Fig. 1). In fact, rainfall increased from 16 UTC to 18 UTC on September 8 over Sagami Bay, corresponding to the eyewall or primary rainband formation south of the typhoon center. In general, it is known that a typhoon changes its structure from an axisymmetric to an asymmetric pattern in mid-latitude, and then it is often transited into an extratropical cyclone. In this regard, the axisymmetrization of Faxai is an unusual phenomenon. In order to understand the role of the ocean and the topography in the axisymmetrization, sensitivity numerical experiments were performed by using a coupled atmosphere-wave-ocean model (Wada et al., 2018).

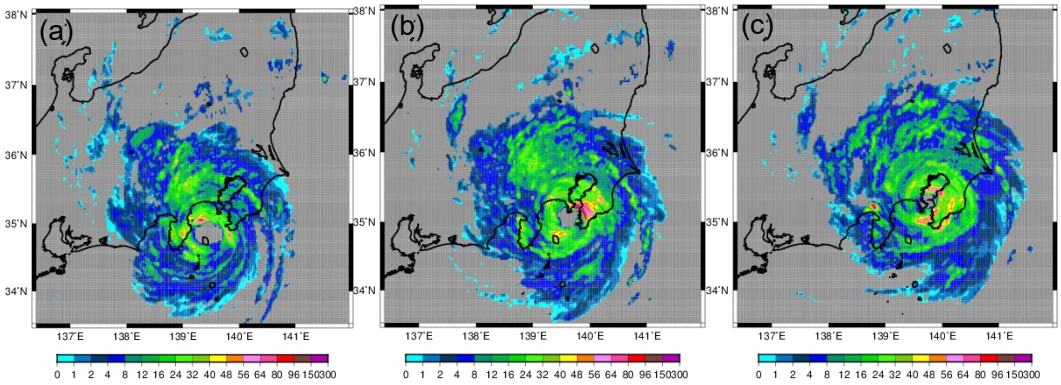

Figure 1 The 1-hour rainfall distribution analyzed every 10 minutes (mm/hour) at (a) 16 UTC, (b) 17 UTC and (c) 18 UTC.

2. Experimental design

Table1 List of numerical simulations

Name	***Model***	***Ocean***	***Topography***
CPL	Coupled NHM-wave-ocean model	2019	Default
CPLAVE	Coupled NHM-wave-ocean model	Climatology	Default
CPL100m	Coupled NHM-wave-ocean model	2019	100m in the Kanto area
CPLizu2	Coupled NHM-wave-ocean model	2019	Twice in the Izu Peninsula

The list of numerical simulations is shown in Table 1. Each initial time was 0000 UTC on September 8. The computational domain was 960 x 1260 km. The number of the vertical layer was 55. The top height was approximately 27 km. The integration time was 36 hours. The time step was 3 seconds for NHM, 18 seconds for the ocean model, and 6 minutes for the ocean surface wave model.

The physical components were exchanged between NHM, the ocean model, and the ocean surface wave model every time step of a model with a longer time step. The Japan Meteorological Agency (JMA) mesoscale objective analysis with horizontal resolution of 5 km and the JMA North Pacific Ocean analysis with horizontal resolution of 0.5° were used for creating atmospheric and oceanic initial conditions and atmospheric lateral boundary conditions. In addition, climatological oceanic averaged data are calculated by using the oceanic reanalysis data from 1982 to 2018 (Usui et al., 2017). When the climatological data are used in the simulation, 'AVE' is added to the end of the experiment name shown in Table 1. In addition, two sensitivity numerical experiments were performed on topography. One was to set the altitude in the Kanto area to 100m, and the other was to set the altitude double in the Izu Peninsula.

3. Results

3.1 Radius of maximum wind speed

Figure 2 shows the time series of simulated maximum surface wind speed and its radius. After around 12UTC on September 8, the simulated maximum surface wind speed greatly increased compared with the Regional Specialized Meteorological Center Tokyo best track maximum surface

wind. It should be noted that the time representativeness of simulated surface winds is less than 1 hour because instantaneous values are used for the analysis of the simulations. Another reason for the large difference in maximum surface winds at the initial time is that there is a large difference between early anasysis and confirmed best track data. While the simulated maximum surface wind increased, the radius certainly reduced in all the four simulations.

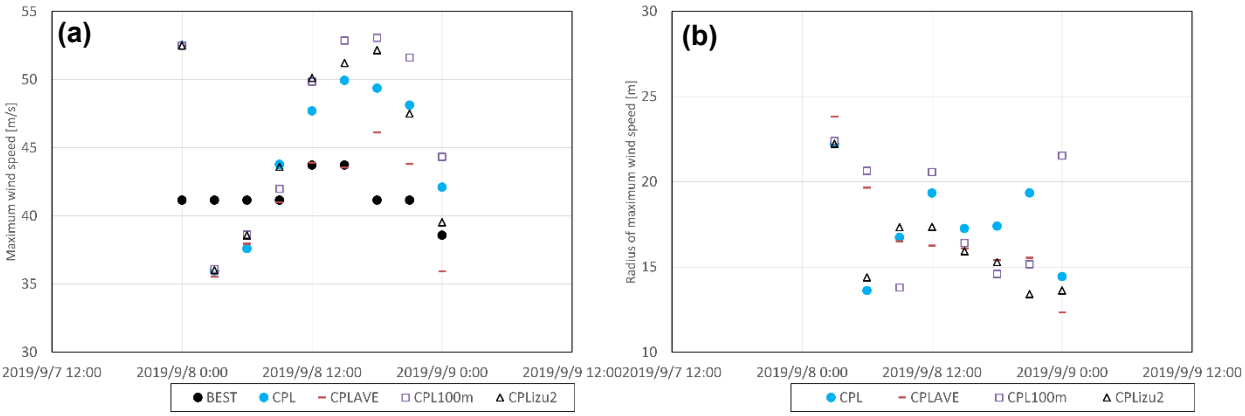

Figure 2 Time series of (a) simulated maximum surface wind speed and (b) simulated radius of the maximum surface wind speed.

3.2 Rainfall distribution

Figure 3 shows the horizontal distributions of 1-hour accumulated rainfall in the four experiments simulated by the coupled model. Rainfall at the eyewall west of the typhoon center ('A') was simulated much more than the analysis shown in Fig. 1. A primary rainband south of the typhoon center ('B') was simulated in the CPLAVE and CPLizu2 experiments although it was not analyzed in Fig. 1a. A rainfall shield northwest of the typhoon center ('C') was not simulated in the CPL100m experiment. These results indicate the effect of oceanic environment represented by the difference between real and climate oceanic conditions on the rainfall amount and that of topography on the rainfall distribution. Without the topography, axisymmetrization of the rainfall pattern in the CPL100m experiment would be more concentric than that in the other experiments. It should be noted that there is a difference in the horizontal distribution of simulated sea surface temperature in between CPLAVE and the other experiments: in the CPLAVE experiment, sea surface cooling was induced by Faxai along the typhoon track, while another sea surface cooling was salient west of Sagami Bay in the other experiments (not shown).

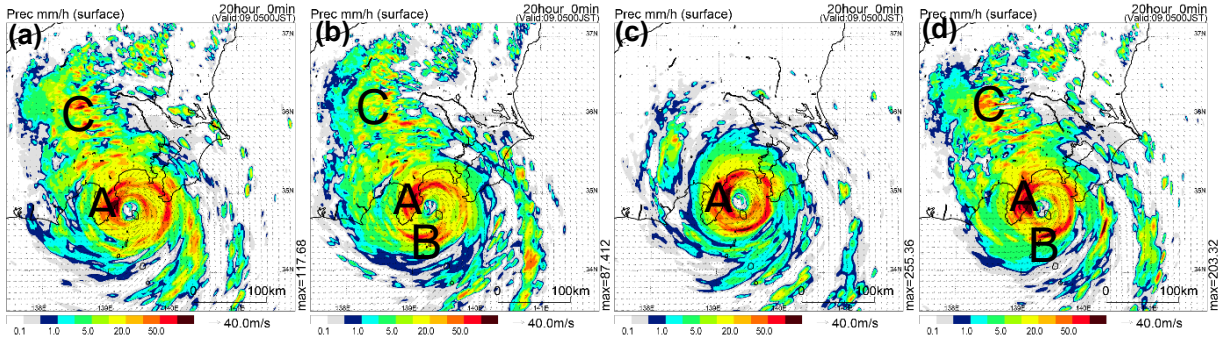

Figure 3 The 1-hour accumulated rainfall distribution simulated by the atmosphere-wave-ocean coupled model in the (a) CPL, (b) CPLAVE, (c) CPL100m and (d) CPLizu2 experiments.

4. Concluding remarks

The coupled model can simulate axisymmetrization regardless of the oceanic initial conditions and topographical setting. In other words, factors that cause the axisymmetrization may be related to another factor such as atmospheric environmental condition and its associated typhoon track.

References

Usui, N, T. Wakamatsu, Y. Tanaka, N. Hirose, T. Toyoda, S. Nishikawa, et al, (2017), Four-dimensional variational ocean reanalysis: a 30-year high-resolution dataset in the western North Pacific (FORA-WNP30). Journal of Oceanography, 73, 205-233.

Wada, A., S. Kanada, and H. Yamada (2018). Effect of air–sea environmental conditions and interfacial processes on extremely intense typhoon Haiyan (2013). Journal of Geophysical Research: Atmospheres, 123, 10379-10405.

Atmosphere-wave-ocean coupled-model simulation on rapid intensification of Typhoon Hagibis (2019)

Akiyoshi Wada

[1]Meteorological Research Institute, Tsukuba, Ibaraki, 305-0052, JAPAN

[1]awada@mri-jma.go.jp

1. Introduction

Typhoon Hagibis (2019) enlarged rapidly its size from its genesis at 18UTC on October 5 to its rapid intensification. After reaching a central pressure of 915 hPa at 12 UTC on October 6, the central pressure lasted 66 hours. The typhoon made landfall in the Izu Peninsula after it was travelling over the ocean where the sea surface temperature exceeded 27 ° C, while maintaining its large size and strong intensity. Extraordinary large amounts of water vapor were transported to the Japanese archipelago while the typhoon was moving north, causing record-breaking heavy rains in eastern Japan and increasing flood damage from river floods. In order to understand the dynamic and thermodynamics of rapid intensification and large size, numerical simulations were performed on Hagibis in the early and rapid intensification phase using the 1-km mesh coupled atmosphere-wave-ocean model (Wada et al., 2018).

2. Experimental design

The list of numerical simulations is shown in Table 1. Each initial time was 0000 UTC on October 6. The computational domain was 1620 x 990 km. The number of the vertical layer was 55. The top height was approximately 27 km. The integration time was 42 hours. The time step was 3 seconds for NHM, 18 seconds for the ocean model, and 6 minutes for the ocean surface wave model.

Table1 List of numerical simulations

Name	*Model*	*Ocean*
NHM	NHM	2019
CPL	Coupled NHM-wave-ocean model	2019
NHMAVE	NHM	Climatology
CPLAVE	Coupled NHM-wave-ocean model	Climatology

The physical components were exchanged between NHM, the ocean model, and the ocean surface wave model every time step of a model with a longer time step. The Japan Meteorological Agency (JMA) global objective analysis with horizontal resolution of 20 km and the JMA North Pacific Ocean analysis with horizontal resolution of 0.5° were used for creating atmospheric and oceanic initial conditions and atmospheric lateral boundary conditions. In addition, climatological oceanic averaged data are calculated by using the oceanic reanalysis data from 1982 to 2018 (Usui et al., 2017). When the climatological data are used in the simulation, 'AVE' is added to the end of the experiment name shown in Table 1. It should be noted that to simulate a strong typhoon, the coverage of sea spray was assumed to be 100% instead of 4% (Wada et al. 2018).

3. Results

3.1 Track and central pressure

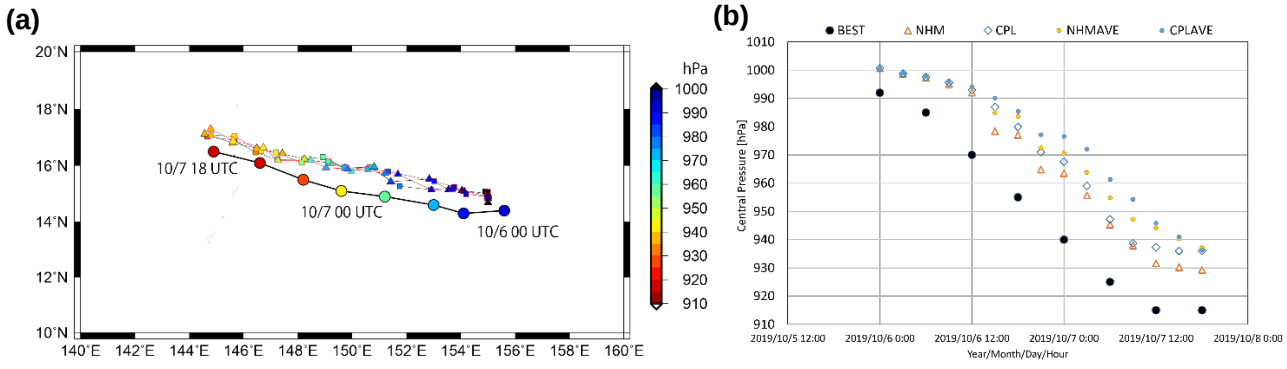

Figure 1 (a) Regional Specialized Meteorological Center (RSMC) Tokyo best track and simulated tracks listed in Table 1 from 00 UTC on October 6 to 18 UTC on October 7 in 2019. (b) Time series of RSMC Tokyo best track central pressure and simulated central pressures listed in Table 1.

Figure 1 shows the simulated tracks and Regional Specialized Meteorological Conter (RSMC) Tokyo best track for comparison. Although the simulated tracks were deflected north, the moving direction west-northwest was well simulated. Although the initial value of the center pressure was higher than that of RSMC best track central pressure, the change in simulated central pressure was reasonable compared with that in RSMC Tokyo best track central pressure. Regarding the impact of difference in the oceanic initial conditions between real-time analysis and climatological mean on the central pressure simulation, the simulated central pressures in the NHM and CPL

experiments tended to be lower than those in the NHMAVE and CPLAVE experiments. In addition, the effect of ocean coupling became clearer as the simulated central pressure decreased. The sea surface temperature underneath the typhoon was hardly cooled over the ocean where the oceanic mixed layer was relatively deep. Therefore, the simulated central pressure could deepen more rapidly and was able to maintain the lowest value since the upper-ocean heat content on October in 2019 was higher than climatological mean (not shown).

3.2 Structural change during rapid intensification

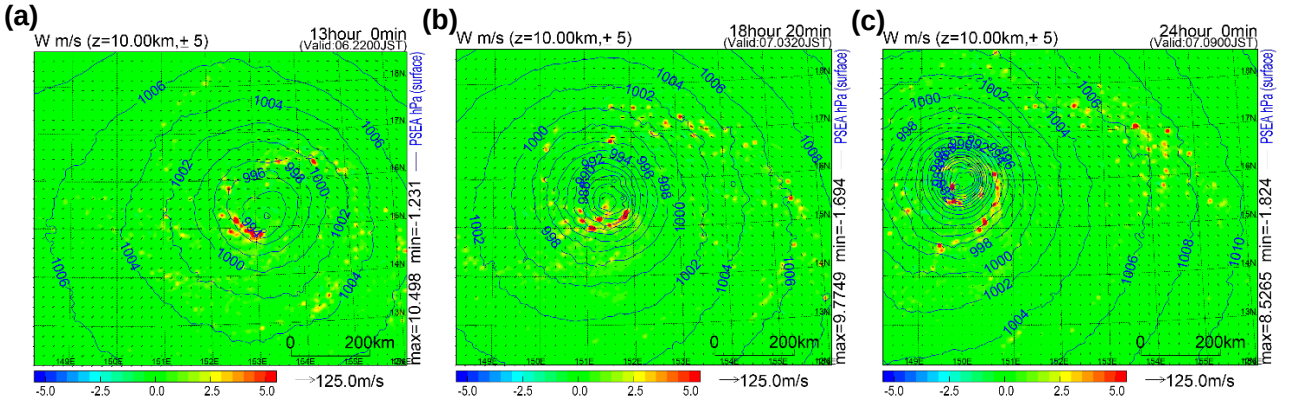

Figure 2 Horizontal distributions of vertical wind velocity (m s^{-1}: colors), horizontal winds at a 10-km height (m s^{-1}: vectors) and sea-level pressure (hPa: contours) at (a) 13-h, (b) 18-h 20-min, and 24-h integration times.

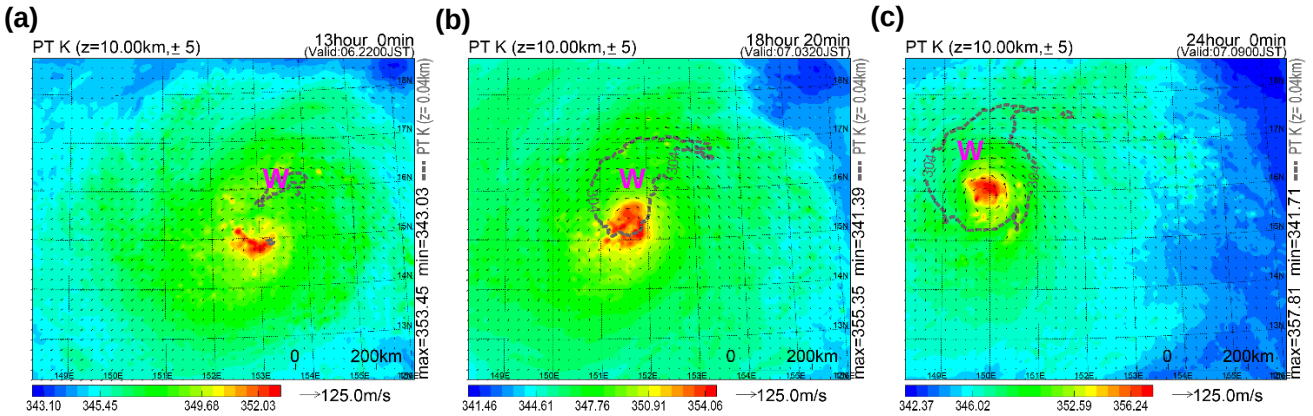

Figure 3 Horizontal distributions of potential temperature (K: colors), horizontal winds at a 10-km height (m s^{-1}: vectors) and surface potential temperature (K: contours) at (a) 13-h, (b) 18-h 20-min, and 24-h integration times.

Figures 2 and 3 show the horizontal distributions of vertical velocity and potential temperature at a 10-km height at 13h, 18h20m and 24h. At the 13-h integration time, the area of upward motion was spirally distributed southwest of the typhoon center where the potential temperature was higher than its surroundings. Apart from the upper warm area, there was a high potential temperature area near the surface northeast of the typhoon center. The near-surface warm area began to overlap with the upper warm area at the 18h20m integration time when the area of upward motion moved spirally south of the typhoon center, and finally the upper warm area was included in the near surface warm area at the 24h integration time. At the time, the central pressure had been rapidly lowering. In addition, another upward-motion area, corresponding to a spiral rainband outside the eyewall was generated.

4. Summary and future subject

The rapid intensification of Typhoon Hagibis (2019) was reasonably simulated in the NHM and CPL experiments. The rapid intensification and the sustenance of the lowest central pressure occurred when Hagibis passed over the ocean where the upper-ocean heat content was higher than the climatological mean. The upward vertical velocity in the upper troposphere contributed to the formation of high potential-temperature area southwest of the typhoon center, whereas high potential temperature area was formed near the surface northeast of the typhoon center. The central pressure lowered rapidly when the high potential temperature area in the upper troposphere was included in the potential-temperature area near the surface. The relationship between the formation of potential-temperature area near the surface and the enlargement of typhoon size is a subject in the future.

References

Usui, N, T. Wakamatsu, Y. Tanaka, N. Hirose, T. Toyoda, S. Nishikawa, et al, (2017), Four-dimensional variational ocean reanalysis: a 30-year high-resolution dataset in the western North Pacific (FORA-WNP30). Journal of Oceanography, 73, 205-233.

Wada, A., S. Kanada, and H. Yamada (2018). Effect of air–sea environmental conditions and interfacial processes on extremely intense typhoon Haiyan (2013). Journal of Geophysical Research: Atmospheres, 123, 10379-10405.

Atmosphere-wave-ocean coupled-model simulation on the effect of Himawari-8 all-sky infrared radiances assimilation on the track simulation of Typhoon Jongdari (2018)

Akiyoshi Wada, Kozo Okamoto

[1]Meteorological Research Institute, Tsukuba, Ibaraki, 305-0052, JAPAN

[1]awada@mri-jma.go.jp

1. Introduction

Typhoon Jongdari was generated around 19.7°N, 136.7°E at 12 UTC on July 24 in 2018. First, the typhoon moved northward and then moved counterclockwise over the ocean south of Japan, and made landfall in Ise City, Mie Prefecture, with a central pressure of 970 hPa and a maximum sustained surface wind speed of 35 m s^{-1}. The Jongdari's track was unusual when compared with the typical typhoon track in July because the unusual track could be influenced by the cut-off of upper cold low. The improvement of the quality of global objective analysis data may serve as understanding of the interaction between the upper cold low and the typhoon vortex and the dynamics of the unusual typhoon track in the framework of the atmosphere-ocean coupled system. Therefore, we applied Himawari-8 all-sky infrared radiances assimilation data for atmospheric initial conditions and numerical simulations were performed by a coupled atmosphere-wave-ocean model and various atmospheric initial and boundary conditions created by different global objective analysis data at different initial times.

2. Experimental design

Numerical simulations were performed by using a nonhydrostatic atmospheric model (NHM) and coupled atmospheric-wave-ocean model (CPL). The list of numerical simulations is shown in Table 1. The horizontal resolution was 3 km and the domain was 3000 x 3000 km. The number of the vertical layer was 55. The top height was approximately 27 km.

Table1 List of numerical simulations

Atmospheric condition	*Model*	*Initial time*
NAPS10 (JMA, 2019)	NHM / CPL	12 UTC on July 25 to
CNT（Geer et al. 2018）	NHM / CPL	12 UTC on July 28
ASR (New product)	NHM / CPL	(6-hour interval)

The atmospheric initial and lateral boundary conditions of the atmospheric model were created by the following three global analysis data, respectively. The experiment ‘NAPS10’ used the global objective analysis data based on the Japan Meteorological Agency (2019). The data is currently available in the operational system in the Japan Meteorological Agency (JMA). The experiment ‘CNT’ used the global objective analysis data calculated based on Geer et al. (2018). The experiment ‘ASR’ used the improved version from the ‘CNT’ global objective analysis data and the assimilation system is under development.

The JMA North Pacific Ocean analysis data with horizontal resolution of 0.5° were used for creating oceanic initial conditions. The initial time is set every 6 hours from 12 UTC on July 25 to 12 UTC on July 28. The integration time was 144 hours. The time step was 3 seconds for NHM, 18 seconds for the ocean model, and 6 minutes for the ocean surface wave model. The physical components were exchanged between NHM, the ocean model, and the ocean surface-wave model every time step of a model with a longer time step. Detail information is described in Wada et al. (2018).

3. Results

3.1 Track simulations

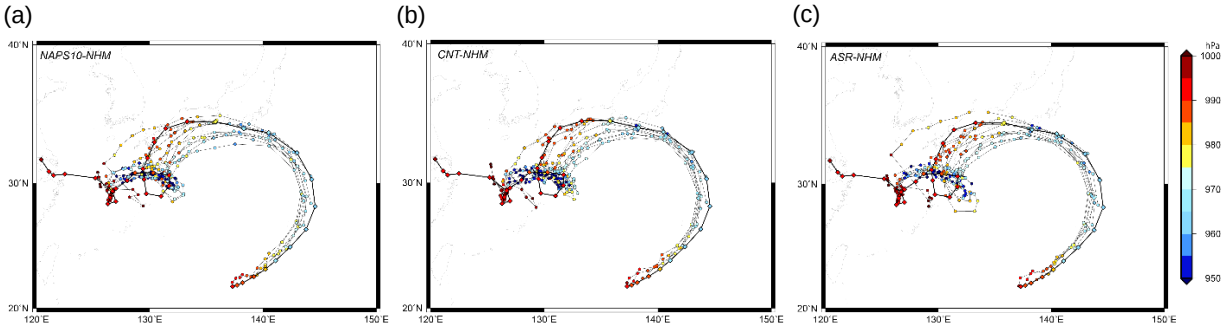

Figure 1 Best track (thick line) and simulated tracks (thin lines) in the (a) NAPS10-NHM, (b) CNT-NHM, (c) ASR-NHM experiments. Colors indicate the best-track central pressure and simulated central pressures plotted every 6 hours.

Figure 1 shows the simulated tracks in the NAPS10-NHM, CNT-NHM, and ASR-NHM experiments together with the Regional Specialized Meteorological Center Tokyo best track data. In almost all the experiments, when

compared with the best track data, the overall tendency of simulated tracks was a westward deviation at the early integration, a southern deviation while moving westward, and an eastern deviation of the counterclockwise track south of Kyushu. This tendency was also found in the results of numerical simulations by the CPL. The impact of the difference between NAPS10, CNT and ASR on the typhoon simulation performed by the NHM and the CPL was found in the difference in simulated tracks and simulated central pressure to some extent but did not lead to the improvement of track simulations significantly.

3.2 Predictability of typhoon track and central pressure

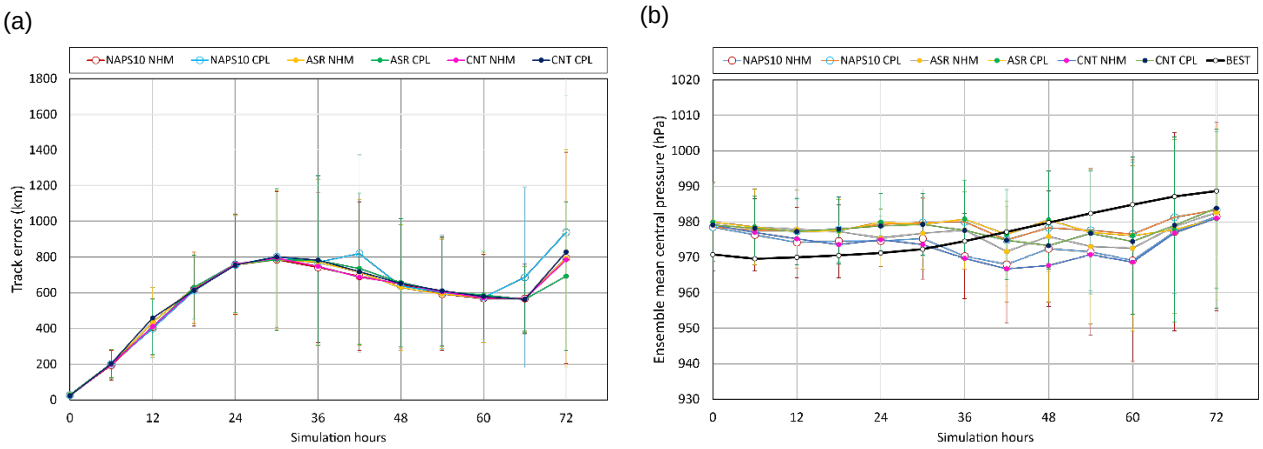

Figure 2 Time series of (a) mean track errors at each integration time (6-hour interval) in each experiment (Table 1) with reference to the best track data and (b) mean best track (thick black line with open circles) and mean simulated central pressure at each integration time (6-hour interval) in each experiment (Table 1). The error bar indicates the standard deviation at each integration time. The mean value is calculated using all simulation results from the initial time every 6 hours from 12 UTC on July 25 to 12 UTC on July 28.

Figure 2 shows the time series of mean simulated track errors and mean simulated central pressures in all the experiments (Table 1). When compared with the best track data, the simulated track errors did not significantly differ between the six experiments, but rather the standard deviation resulted from the difference of the initial time becomes large in the latter of the integration. However, at the 72-h integration time, the simulated track was improved in the ASR-CPL experiment, while the simulated track in the NAPS-CPL experiment became worst.

Regarding the simulated central pressure, the NHM experiment shows a systematic tendency to lower the central pressure in the latter half of the integration. Although the central pressure at the initial time did not match that of the best track data, simulated central pressure by the NHM was relatively low even at the early integration, which affected the relatively low value of simulated center pressure even in the latter half of the integration. The standard deviation of simulated central pressure resulted from the difference of the initial time became large in the latter of the integration. The result suggests that both the effect of ocean coupling and the difference of the atmospheric initial condition between initial times had a greater effect on Jongdari's simulation than the difference of the methodology to create global objective analysis data.

4. Concluding remarks

This study investigated the impacts of the methodology to create the global objective analysis data on the simulation of Typhoon Jongdari (2018) by using a nonhydrostatic atmosphere model and its coupled atmosphere-wave ocean model with three kinds of global objective analysis data at different initial times. Both ocean coupling and differences in atmospheric initial and boundary conditions between initial times had a greater impact on simulated tracks and central pressures than the difference of the global atmospheric data assimilation method. It should be noted that Himawari-8 all-sky infrared radiances assimilation is currently under development. In order to understand the dynamics of unusual Jongdari's track, it is necessary to evaluate the steering flow and the interaction between the upper cold low and the typhoon vortex by using the different global objective analysis data and its simulation results. This is a subject in the future.

References

Geer, AJ, Lonitz, K, Weston, P, et al. (2018), All sky satellite data assimilation at operational weather forecasting centres. Quarterly Journal of the Royal Meteorological Society, 144, 1191‐1217.

Japan Meteorological Agency (2019), Outline of the operational numerical weather prediction at the Japan Meteorological Agency. Appendix to WMO Technical Progress Report on The Global Data Processing and Forecasting SYSTEM (GDPFS) and Numerical Weather Prediction (NWP) Research, Japan Meteorological Agency, Tokyo, Japan, 229 pp. (Available at https://www.jma.go.jp/jma/jma-eng/jma-center/nwp/outline2019-nwp/index.htm, accessed 19 Feb 2020)

Usui, N, T. Wakamatsu, Y. Tanaka, N. Hirose, T. Toyoda, S. Nishikawa, et al, (2017), Four-dimensional variational ocean reanalysis: a 30-year high-resolution dataset in the western North Pacific (FORA-WNP30). Journal of Oceanography, 73, 205-233.

Wada, A., S. Kanada, and H. Yamada (2018). Effect of air–sea environmental conditions and interfacial processes on extremely intense typhoon Haiyan (2013). Journal of Geophysical Research: Atmospheres, 123, 10379-10405.